Delineation of Subsurface Structures using Seismic Refraction Tomographic Inversion in Wadi Al-Dawasir, South Saudi Arabia

Nouh Alotaibi
Geophysics, College of Science, King Saud University, Saudi Arabia
nsalotaibi@kacst.edu.sa (corresponding author)

Ahmed Metwally
Geophysics Department, Faculty of Science, Cairo University, Egypt
ahmed_mohsen_geo@yahoo.com

Received: 22 May 2024 | Revised: 25 June 2024, 8 July 2024, and 14 July 2024 | Accepted: 15 July 2024

Licensed under a CC-BY 4.0 license | Copyright (c) by the authors | *DOI: https://doi.org/10.48084/etasr.7915*

ABSTRACT

The main objective of this paper is to delineate the subsurface structures, especially faults, in Al Haddar, Wadi Al-Dawasir area which is a part of the Sulayyimah Quadrangle, South Saudi Arabia using non-linear seismic refraction tomographic inversion. No major structures or faults are observed from the surface geological studies, while most of the area is covered with sand dunes and recent quaternary deposits. The purpose of the current research is to use the seismic method, which has been widely deployed in detecting and mapping subsurface features, to delineate the subsurface structures utilizing the 2-D seismic refraction travel-time tomographic inversion technique. The main advantages of travel time tomography are that it is a nondestructive technique, it provides a velocity model for the subsurface and delineates the subsurface faults with very high accuracy without involving drilling or trenching. The seismic data were acquired employing the most advanced and up-to-date instruments for high-resolution investigation. The system consists of the source, which is a vibrator (Vibroseis), sensors (receivers or geophones), and the acquisition system. A 40 Hz vertical geophone Model GS-20DH was used as the receiver, Strata Visor with geodes was put into service as the acquisition system, and end-on spread was installed by utilizing 112 geophones, while the source is offset 10 m away from the seismic line. The length of the acquired seismic line was 4.5 km. The final velocity tomogram is graphically presented as a 2-D grid of pixels, where each pixel contains the model parameters of interest such as the velocity value or its reciprocal value known as slowness. The travel-time tomography was able to provide a velocity model for the subsurface and delineate the subsurface faults with high accuracy.

Keywords-Wadi Al-Dawasir; seismic refraction; travel-time tomography; subsurface faults

I. INTRODUCTION

The purpose of this paper is to delineate and identify shallow subsurface faults via seismic refraction tomography. Several wave forms captured during a seismic survey are recorded. The first-arrival travel-times of refractions can be inverted to construct the subsurface velocity model. The P-velocity tomogram is the name given to the resulting velocity model, which is used to detect the positions of near-surface faults with sharp velocity contrasts. The study area is located within the Sulayyimah quadrangle, between longitudes 45°30'13.55" - 45°32'54.59" east and latitudes 21°43'54.78" - 21°46'55.29" north in the southeast of the Najd province of Saudi Arabia (Figure 1). The western fringe of the Sulayyimah quadrangle is an area of Proterozoic crystalline basement rocks at an altitude of 700-800 m. The rest of the Sulayyimah quadrangle is underlain by Phanerozoic sedimentary covers that dip gently away from the basement to an altitude of 600 m at its eastern edge. The basement rocks of the southern Arabian Shield are interpreted to have been formed in a 700 – 800-Ma-oldensimatic island arc [1-3]. These rocks contain highly metamorphosed and deformed succession of andesitic meta-volcanic rocks and inter-bedded volcanic clastic meta-sedimentary rocks. The Proterozoic domain of the Sulayyimah quadrangle consists of a peneplain covered by extensive spreads of eolian sand. The northern part is slightly higher and has a more marked relief than the southern part [4]. The Phanerozoic domain comprises a vast monocline dipping gently eastward at 1-2 degrees. The Phanerozoic rocks in the Sulayyimah quadrangle are contained in a monoclinal structure with a strike of N 20-30° E and an average dip of 1° to the east. The observed faults in the Phanerozoic rocks have a vertical throw of only about 1 m. The major fault detected in the Sulayyimah quadrangle is the N 70° E striking Al Haddar fault.

A second fault visible in Tuwayq escarpment at Khashm Abu Al Jiwar is connected with the Al Haddar fault. According to [4], Al Haddar fault probably represent the trace of a deep fault which affects the basement and whose existence is manifested by the thickness and facies variations in the sedimentary deposits and by later reactivation.

Fig. 1. The Arabian plate with the study area delineated by the red square.

A second regional lineament is shown up by the morphology between Khashm al Mukassar, Wadi Al Shutbah, and Wadi al Maqran. Its orientation is N 70° W, which is similar to the Najd fault system that affects the basement [4]. Some joints appear to have resulted from readjustments of the sedimentary cover, without displacement, to basement movements, which are at least post-Jurassic. According to [5], they are related to the development of the regional monoclinal structure. The southeastward movement along the wrench faults brought this structural unit to a higher position than the surrounding areas to the north and south; hence the name Southern Najd Uplift emerged. The Southern Najd Uplift reached its form through several tectonic phases. The main phase involves very considerable vertical movements before the Pre-Khuff unconformity. It has been demonstrated that tectonic movements resulting in dislocations disappeared after the Triassic rejuvenation [6-8].

In the study area no major faults could be recognized from the surface geology. Most of the area is covered with sand dunes and recent quaternary deposits, as depicted in Figure 2. The Phanerozoic rocks underlie most of the Sulayyimah quadrangle form part of the west edge of the Arabian sedimentary basin and range at the age from the late Permian to the late Cretaceous, as portrayed in Table I. The stratigraphic column represented in Table I illustrates the Phanerozoic rocks in the Sulayyimah quadrangle including the chronostratigraphic and lithostratigraphic units for the study area.

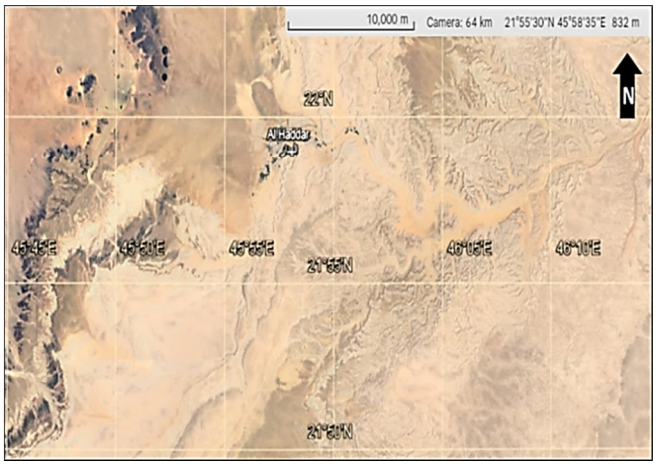

Fig. 2. Landsat image from Google Earth of the study area showing the covering sand dunes and the recent quaternary deposits. © Airbus, CNES/Airbus, Maxar Technologies.

TABLE I. STRATIGRAPHIC COLUMN OF THE PHANEROZOIC ROCKS IN THE SULAYYIMAH QUADRANGLE MODIFIED AFTER [9-12]

Choronostratigraphic units			Lithostratigraphic units
System	**Age (Ma)**	**Series**	**Formation Member**
Creataceous	140	Campanian	Aruma
		Cenomanian	Wasia
		Alpian	Biyadh
		Aptian	Buwaib
		Neocomian	Yamama
			Sulaiy
Jurassic	204	Upper	Haith
			Arab
			Jabailah
			Hanifa
			Tuwatq mountain
		Middle	Dahruma
		Lower	Marat
Triassic	250	Upper	Minjur
		Middle	Jilh
		Lower	Sudair
Permian	290	Upper	Khuff / Unayzah
		Lower	
Carboniferous	360	Upper	
Unconformity			
Proterozoic Basement			

II. MATERIALS AND METHODS

A. Seismic Data Acquisition

A 2D seismic line of 4.5 km long was acquired across the survey area. The recording system consisted of three units: (1) the source unit responsible for positioning and activating the surface-energy sources, (2) the jug hustlers who lay out the cables, place the geophones in their proper locations, and connect them to the cables, and subsequently pick up the geophones and cables, and (3) the recording unit that does the actual recording of the signal. The layout of the seismic lines determines the positions and elevations of both the source points and the geophone groups by using GPS Trimble equipment. Figure 3 shows the elevation contour map with the receiver (geophone) locations projected on it.

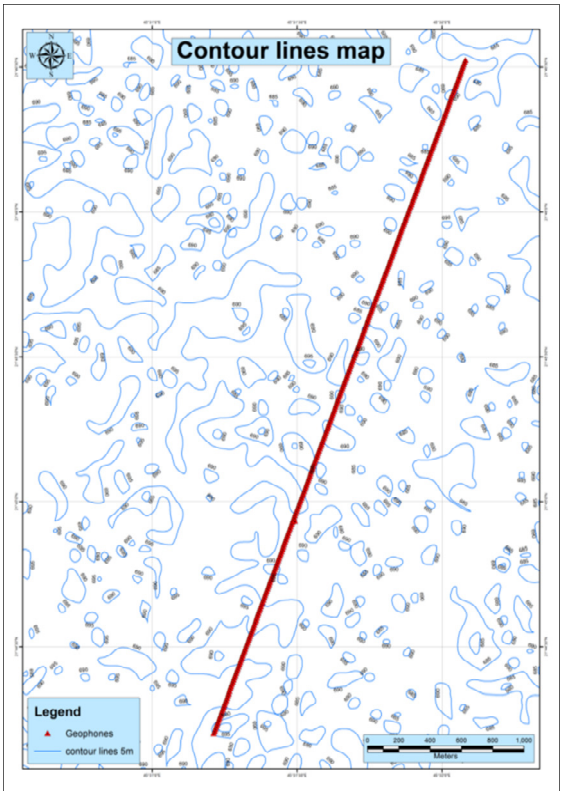

Fig. 3. Elevation contour map with the receiver (geophone) locations projected.

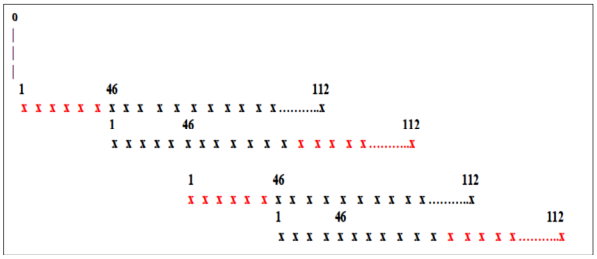

Fig. 4. Seismic spread used during the survey, where the (x) symbol represents the source and geophone-group center locations.

Fig. 5. Vibroseis used in the survey as the seismic source.

End-on spread (the relative locations of source and the center of geophone groups used to record the reflected energy) was conducted by utilizing 112 geophones and the source was offset 10 m away from the seismic line (Figure 4). Figure 5 displays the Vibroseis truck used as the energy source. The sweep start frequency is 10 Hz, and the end frequency is 300 Hz. The total time taken to input this range of frequencies here is 4.0 s. An amplitude taper was placed on each end of the sweep to ease the strain on the equipment 0.05 s. After 3 sweeps at each point the data were stacked automatically to improve signal-noise-ratio. Vertical geophone Model GS-20DH of 40 HZ frequency was utilized as part of a 112 channel station (Figure 6). In areas where the coupling was poor due to sand dunes, a small hole was dug to hit sediments of greater compaction. Table II summarizes the acquisition parameters and the information about the source, receiver, and the recording instrument used in the seismic experiment.

Fig. 6. A 40 HZ geophone layout in which a small whole is dug for better coupling.

TABLE II. ACQUISITION PARAMETERS USED IN THE FIELD SURVEY

Spread		**Source**		**Receiver**		**Instrument**	
Type	Off-end	**Type**	Vibroseis	**Type**	Geo-phone	**Type**	Strata-Visor
No. of traces	112	**Model**	Mini IVI	**Model**	GS20	**Sample interval**	0.5 ms
Geophone interval	15 m	**Sweep**	Linear up-sweep	**Freq.**	40 HZ	**Gain**	36 dB
Source interval	15 m	**Band width**	30-300 HZ	**Damping**	0.70	**Sweep length**	4 s, 2 s
Fold	56	**No. of sweeps**	3	**Spacing**	15 m	**Record length**	6 s

B. Travel-Time Tomography

Travel-time tomography is a standard methodology for reconstructing the subsurface velocity distribution from first-arrival travel-times [13-19], where velocities are updated by an iterative method such as the SIRT technique [20]. The tomography method consists of a number of steps. First, an initial velocity model is estimated from the x-t slope of the first-arrival in the seismograms. The travel-times are then computed from the starting model by a finite-difference solution to the Eikonal equation [21]. In this case, the data misfit function can be defined as:

$$\in = \frac{1}{1}\sum(t_i^{obs} - t_i^{cal})^2 \quad (1)$$

where the summation is over the i^{th} raypath, t_i^{obs} is the associated first arrival travel-time pick, and t_i^{cal} is the calculated travel-time. The j^{th} gradient γ_j of the misfit function is defined by:

$$\gamma_j = \frac{\delta_\epsilon}{\delta_{s_j}} = \sum \delta t_j \frac{\delta t_j}{\delta s_j} = \sum \delta t_i \; l_{ij} \qquad (2)$$

where δt_i is the travel-time residual, δs_j is the slowness in the j^{th} cell, and l_{ij} is the segment length of the i^{th} ray that visits the j^{th} cell. The slowness model is iteratively updated by a gradient optimization method (e.g. steepest descent). Figure 7 summarizes the workflow applied for the travel-time inversion to finally get the final velocity tomogram.

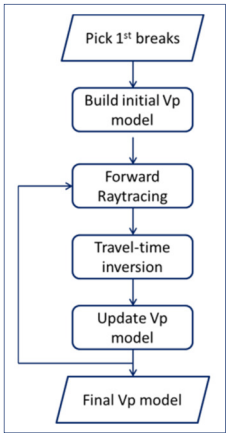

Fig. 7. Workflow for travel-time tomographic inversion.

III. PICKING AND QUALITY CONTROL

A. First-Break Picking

Picking the first arrivals in this dataset was straight forward due to the used source. The first breaks are easily identified as evidenced in Figures (8-11). A tracker was deployed to manually refine the bad picks in common shot gathers.

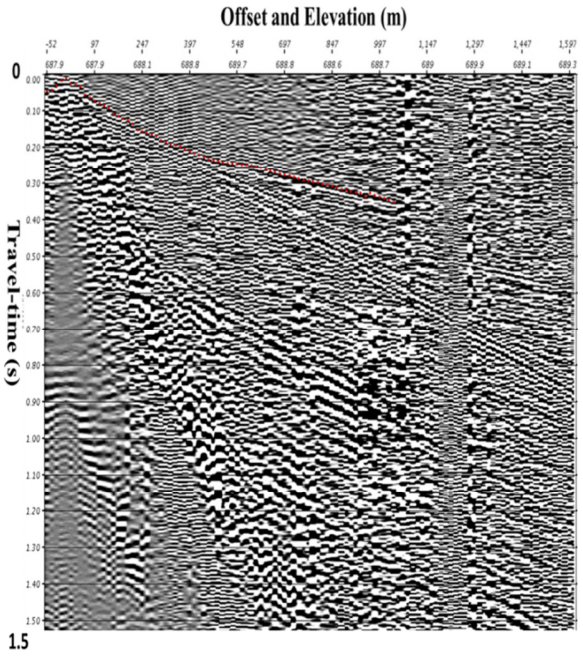

Fig. 8. Shot record with the first break picks for shot no.5.

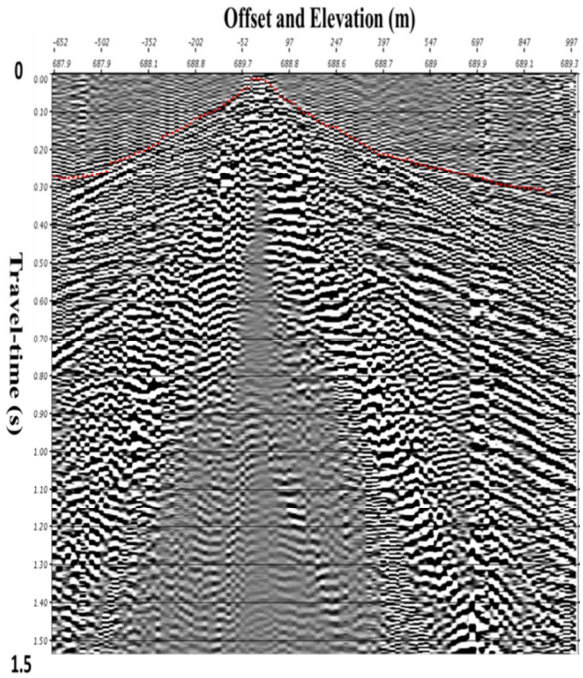

Fig. 9. Shot record with the first break picks for shot no.45.

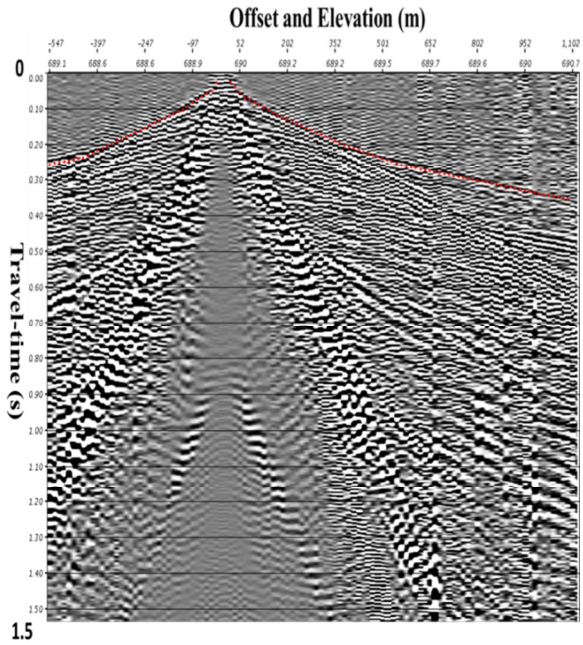

Fig. 10. Shot record with the first break picks for shot no.86.

B. QC Geometry and Bad Picks Refining

After picking the first breaks, the Reciprocal Error QC plot was deployed to check the picks and geometry for the first time. In theory, the reciprocity principal states that the interchanging of the shot and receiver locations does not alter the travel-times. The reciprocal error is the difference between the picked first arrival from the source to the receiver and the receiver to the source.

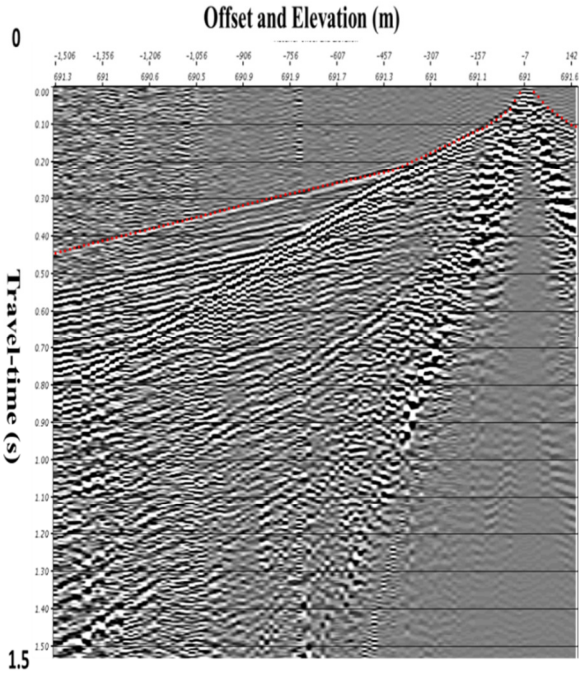

Fig. 11. Shot record with the first break picks for shot no. 299.

In general, the maximum reciprocal error should be less than 20 ms and the average of the reciprocal errors for all shots should be around 10 ms. However, in practice, errors are often caused by geometry or picking error. In this case, the utility indicates the reciprocal error range for all the first breaks and how they are distributed, as can be seen in Figure 12. The X and Y coordinates demonstrate the geometry spread in meters.

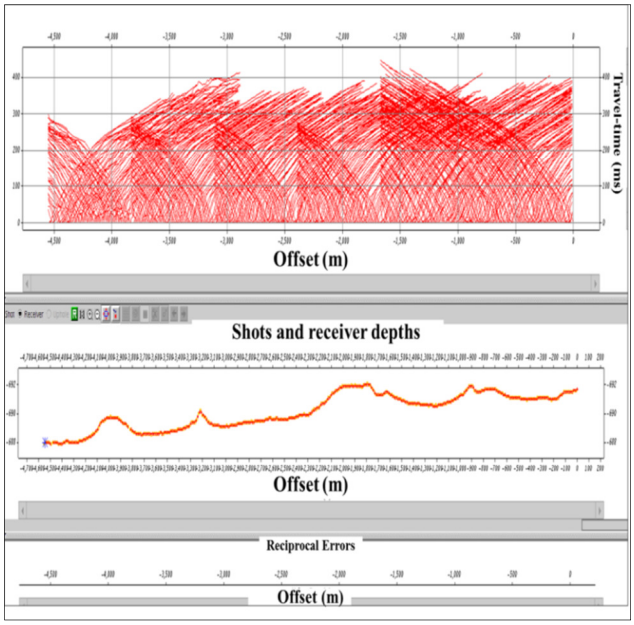

Fig. 12. Travel-time display (top), shot (red) and receiver (yellow) coordinates (middle), RMS reciprocal error for each shot (bottom) with almost no errors.

C. Building the Initial Velocity Model

All the travel-times are displayed together in shot offsets. The color represents data repeatability. Then, this study will start picking a few refraction turning points on the shot offset display curves. The 1-D analytical velocity solutions will be derived from the picked turning points, which will be used to create the 2-D initial velocity model for the travel-time tomography, as observed in Figure 13. The 2-D initial velocity model (Figure 14) is created to start the inversion for travel-time tomography, where the model size is determined by the geometry range and the 1-D model depth and the size of the model square cell is set to half of the receiver spacing.

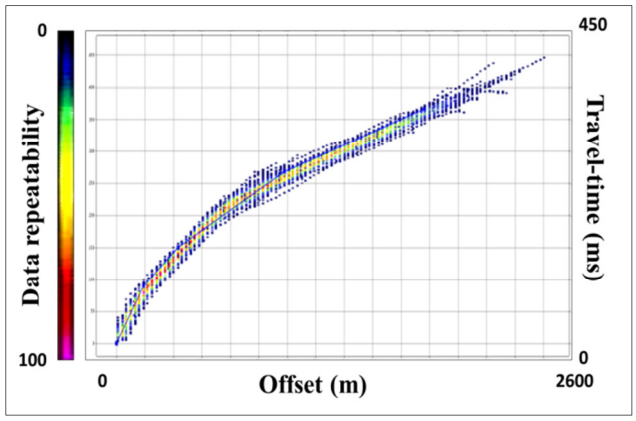

Fig. 13. 1-D velocity solutions used to create the 2-D velocity model to be used as the starting model for the travel-time inversion. The color bar represents the data repeatability.

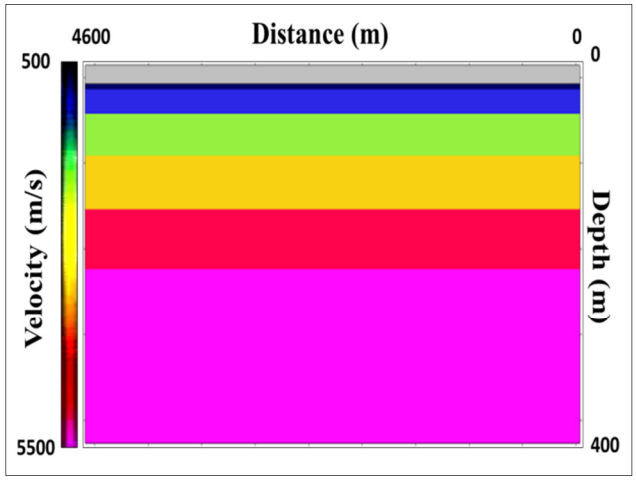

Fig. 14. The 2-D initial velocity model to be used as the starting model for the travel-time inversion.

D. Ray-Tracing & Travel-Time Tomographic Inversion

The travel-time tomography is carried out through a number of steps. First, an initial velocity model is estimated from the x-t slope of the first arrival in the seismograms. The travel-times are then computed from the starting model by a finite-difference solution to the Eikonal equation and the data misfit function is calculated.

Fig. 15. RMS misfit function vs. number of iterations.

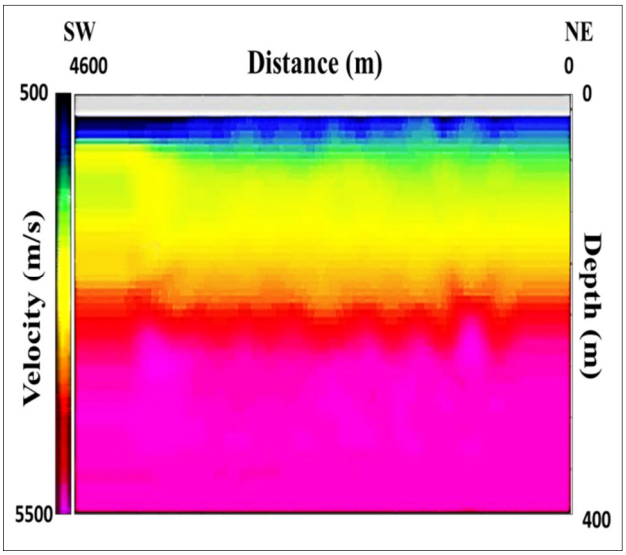

Fig. 16. Final velocity tomogram after six iterations.

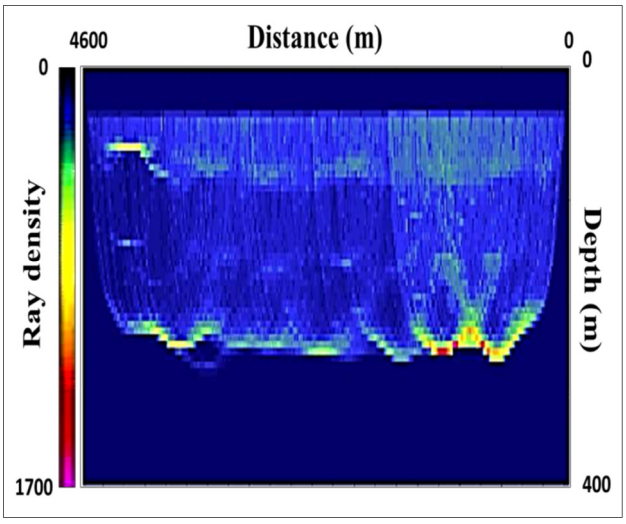

Fig. 17. Ray-tracing for the 2-D travel-time inversion.

Then, the velocity model is updated by an iterative method, where the output velocity model of each iteration is used as the input to the next iteration until the solutions converge and the RMS error reaches minimum. In this case, after six iterations the RMS becomes almost constant (Figure 15) and the inversion is done. The output is the final velocity tomogram (Figure 16). The ray-path density image after ray-tracing from the 2-D travel-time inversion can be seen in Figure 17. From the 2-D travel-time tomogram, we can identify major normal faults, as shown in Figure 18.

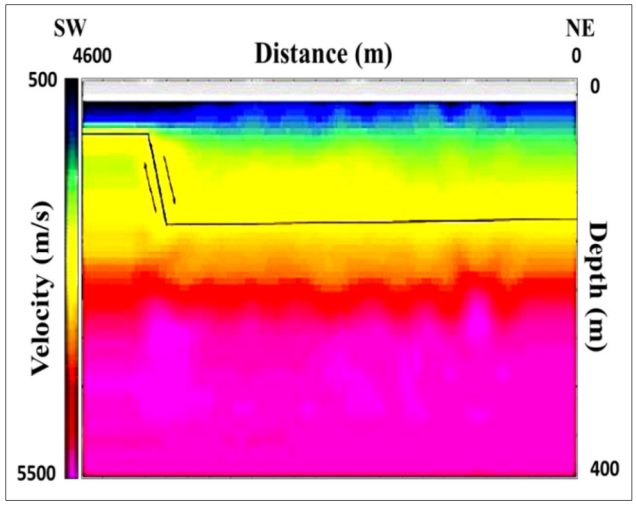

Fig. 18. Seismic refraction travel-time tomogram showing the interpreted subsurface normal fault in the study area.

IV. RESULTS AND DISCUSSION

In this paper, non-linear seismic refraction travel-time tomography was applied to construct the travel-time tomogram. The tomography method consists of a number of steps. First, an initial velocity model was estimated from the x-t slope of the first-arrival in the seismograms. The travel-times were then computed from the starting model by a finite-difference solution to the Eikonal equation. The slowness model was iteratively updated by a gradient optimization method (e.g. steepest descent) to finally get the final velocity tomogram, which was easily interpreted to identify the shallow subsurface structures and faults. The nonlinear refraction travel-time tomography method of [22] was used. This technique includes three main steps: (1) the forward ray-tracing method, (2) the inversion approach that fits travel-time curves, and (3) a nonlinear method for uncertainty analysis. From the generated travel-time tomographic and the velocity distribution of the subsurface, the major normal fault in the study area was identified (Figure 18).

The main advantage of the seismic methods and the travel time tomography is that they provide a velocity model for the subsurface and delineate the subsurface faults with a very accurate and nondestructive technique without the need of drilling or trenching after appropriate processing and interpretation [23-25]. Without altering the natural ground condition, seismic refraction tomography offers the necessary velocity model and subsurface structures [26-29]. The seismic

refraction tomography is a geophysical method that provides the cross-sectional picture along the profile by using the soils' response to the energy from the external source [30-32]. It deploys the inversion technique to obtain the 2D velocity depth profile [33-35].

V. CONCLUSION

The main objective of this paper is to delineate the subsurface faults using seismic refraction tomographic inversion in Al Haddar, Wadi Al-Dawasir Area which is a part of the Sulayyimah Quadrangle, South Saudi Arabia. Non-linear seismic refraction travel-time tomography was applied to construct the travel-time tomogram. The challenging part of this research was to detect the presence of the subsurface faults and structures without any surface geological evidences, as most of the area is covered with sand dunes and recent quaternary deposits. On the final velocity tomogram, a major normal fault could be easily detected which could not be recognized from the surface geology. The travel-time tomography proved to be a very effective method in delineating the subsurface structures, especially faults. The non-linear travel time tomography was able to provide a velocity model for the subsurface and delineate the subsurface faults with very high accuracy and without the need of drilling or trenching.

VI. RECOMMENDATIONS AND FUTURE WORK

As a recommendation, a 3D seismic survey could be conducted as future work on the same area and a 3D refraction travel-time tomogram could be generated to construct a better model for the subsurface, while subsurface faults and other structures would be easily recognized.

REFERENCES

[1] D. L. Schmidt, D. G. Hadley, and D. B. Stoeser, "Late Proterozoic Crustal History of the Arabian Shield, Southern Najd Province, Kingdom of Saudi Arabia," *Inst. Appl. Geol., Bull.*, no. 3, pp. 41–58, 1979.

[2] W. Greenwood and S. A. M. al-ʻĀmmah li-Shuʻūn al-Zayt wa-al-Maʻādin, "Precambrian geologic history and plate tectonic evolution of the Arabian shield," 1980, [Online]. Available: https://www.semanticscholar.org/paper/Precambrian-geologic-history-and-plate-tectonic-of-Greenwood-wa-al-Ma%CA%B9%C4%81din/ccf22d6004c1546178083b8cca73e5507bb7adfc.

[3] W. R. Greenwood, D. B. Stoeser, R. J. Fleck, and J. S. Stacey, "Late Proterozoic island-arc complexes and tectonic belts in the southern part of the Arabian Shield, Kingdom of Saudi Arabia," United States Geological Survey, Reston, VA, USA, Open-File Report 83-296, 1983.

[4] D. Vaslet *et al.*, *Explanatory notes to the geologic map of the Sulayyimah Quadrangle, Sheet 24 H, Kingdom of Saudi Arabia*. Jeddah, Saudi Arabia: Saudi Arabian Deputy Ministry for Mineral Resources, 1984.

[5] J. M. Moore, "Volcanogenic mineralization and a rhyolite dome in the Arabian Shield," *Mineralium Deposita*, vol. 13, no. 1, pp. 123–129, Mar. 1978, https://doi.org/10.1007/BF00202912.

[6] H. J. Al-Faifi, "Evaluation of groundwater resources in Wajid aquifer in Wadi Dawasir area Southern Saudi Arabia using computer simulation," M.S. thesis, King Saud University, Riyadh, Saudi Arabia, 2005.

[7] W. Bosworth, P. Huchon, and K. McClay, "The Red Sea and Gulf of Aden Basins," *Journal of African Earth Sciences*, vol. 43, no. 1, pp. 334–378, Oct. 2005, https://doi.org/10.1016/j.jafrearsci.2005.07.020.

[8] *Italconsult, Water and Agricultural Development studies for Area IV, Eastern Province, Saudi Arabian*. Unpublished Report to the Ministry of Agriculture and Water, Riyadh, Kingdom of Saudi Arabia, 1969.

[9] M. Al-Ahmadi, "Hydrogeology of the Saq Aquifer Northwest of Tabuk, Northern Saudi Arabia," *Journal of King Abdulaziz University-Earth Sciences*, vol. 20, no. 1, pp. 51–66, 2009, https://doi.org/10.4197/Ear.20-1.4.

[10] H. S. Edgell, *Regional Stratigraphic Relationships of Arabia in Exploration for Oil and Gas. In, Short Course on Hydrocarbon Exploration*. Dhahran, Saudi Arabia: King Fahd University of Petroleum and Minerals, 1987.

[11] A. A. Al-Aswad and A. M. Al-Bassam, "Proposed hydrostratigraphical classification and nomenclature: application to the Palaeozoic in Saudi Arabia," *Journal of African Earth Sciences*, vol. 24, no. 4, pp. 497–510, May 1997, https://doi.org/10.1016/S0899-5362(97)00077-8.

[12] A. M. Al-Bassam, M. E. Al-Dabbagh, and M. T. Hussein, "Application of a revised hydrostratigraphical classification and nomenclature to the Mesozoic and Cenozoic succession of Saudi Arabia," *Journal of African Earth Sciences*, vol. 30, no. 4, pp. 917–927, May 2000, https://doi.org/10.1016/S0899-5362(00)00060-9.

[13] M. A. E. Hameedy, W. M. Mabrouk, S. Dahroug, M. S. Youssef, and A. M. Metwally, "Role of Seismic Refraction Tomography (SRT) in bedrock mapping; case study from industrial zone, Ain-Sokhna area, Egypt," *Contributions to Geophysics and Geodesy*, vol. 53, no. 2, pp. 111–128, Jun. 2023, https://doi.org/10.31577/congeo.2023.53.2.2.

[14] A. Metwally, S. Hanafy, B. Guo, and M. Kosmicki, "Imaging of subsurface faults using refraction migration with fault flooding," *Journal of Applied Geophysics*, vol. 143, pp. 103–115, Aug. 2017, https://doi.org/10.1016/j.jappgeo.2017.05.003.

[15] W. J. Lutter, R. L. Nowack, and L. W. Braile, "Seismic imaging of upper crustal structure using travel times from the PASSCAL Ouachita Experiment," *Journal of Geophysical Research: Solid Earth*, vol. 95, no. B4, pp. 4621–4631, 1990, https://doi.org/10.1029/JB095iB04p04621.

[16] G. Nolet, *Seismic Tomography: With Applications in Global Seismology and Exploration Geophysics*. Dordrecht, Netherlands: D. Reidel, 1987.

[17] D. Aldridge and D. Oldenburg, "Two-Dimensional Tomographic Inversion With Finite-Difference Traveltimes," *Journal of Seismic Exploration*, vol. 2, no. 3, pp. 257–274, Jan. 1993.

[18] C. J. Ammon and J. E. Vidale, "Tomography without rays," *Bulletin of the Seismological Society of America*, vol. 83, no. 2, pp. 509–528, Apr. 1993, https://doi.org/10.1785/BSSA0830020509.

[19] T. Nemeth, E. Normark, and F. Qin, "Dynamic smoothing in crosswell traveltime tomography," *GEOPHYSICS*, vol. 62, no. 1, pp. 168–176, Jan. 1997, https://doi.org/10.1190/1.1444115.

[20] P. Gilbert, "Iterative methods for the three-dimensional reconstruction of an object from projections," *Journal of Theoretical Biology*, vol. 36, no. 1, pp. 105–117, Jul. 1972, https://doi.org/10.1016/0022-5193(72)90180-4.

[21] F. Qin, Y. Luo, K. B. Olsen, W. Cai, and G. T. Schuster, "Finite-difference solution of the eikonal equation along expanding wavefronts," *Geophysics*, vol. 57, no. 3, pp. 478–487, Mar. 1992, https://doi.org/10.1190/1.1443263.

[22] J. Zhang and M. N. Toksöz, "Nonlinear refraction traveltime tomography," *GEOPHYSICS*, vol. 63, no. 5, pp. 1726–1737, Sep. 1998, https://doi.org/10.1190/1.1444468.

[23] A. Younesi, R. Rahmani, J. Jaafari, and Y. Mahdavi, "Environmental Risk Assessment and Management in Oil Platform Construction Phase Activities: A Case Study," *Engineering, Technology & Applied Science Research*, vol. 7, no. 3, pp. 1658–1663, Jun. 2017, https://doi.org/10.48084/etasr.1127.

[24] S. Eladj, T. K. Lounissi, M. Z. Doghmane, and M. Djeddi, "Lithological Characterization by Simultaneous Seismic Inversion in Algerian South Eastern Field," *Engineering, Technology & Applied Science Research*, vol. 10, no. 1, pp. 5251–5258, Feb. 2020, https://doi.org/10.48084/etasr.3203.

[25] E. Roshdy, W. Mabrouk, and A. Metwally, "Application of Noise Attenuation on 2D Shallow Offshore Seismic Reflection Data: A Case Study from the Baltic Sea," *Engineering, Technology & Applied Science Research*, vol. 12, no. 2, pp. 8431–8434, Apr. 2022, https://doi.org/10.48084/etasr.4748.

[26] I. N. Azwin, R. Saad, and M. Nordiana, "Applying the Seismic Refraction Tomography for Site Characterization," *APCBEE Procedia*, vol. 5, pp. 227–231, Jan. 2013, https://doi.org/10.1016/j.apcbee.2013.05.039.

[27] E. Cardarelli, M. Cercato, A. Cerreto, and G. D. Filippo, "Electrical resistivity and seismic refraction tomography to detect buried cavities," *Geophysical Prospecting*, vol. 58, no. 4, pp. 685–695, May 2010, https://doi.org/10.1111/j.1365-2478.2009.00854.x.

[28] S. Maraio, P. Bruno, G. Testa, P. Tedesco, and G. Izzo, "Application of seismic refraction tomography to detect anthropogenic buried cavities in Province of Naples," in *GNGTS 2014*, Trieste, Italy, 2014, pp. 90–94.

[29] J. R. Sheehan, W. E. Doll, and W. A. Mandell, "An Evaluation of Methods and Available Software for Seismic Refraction Tomography Analysis," *Journal of Environmental and Engineering Geophysics*, vol. 10, no. 1, pp. 21–34, Mar. 2005, https://doi.org/10.2113/JEEG10.1.21.

[30] C. C. Chiemeke and I. B. Osazuwa, "Assessment of the Response of Seismic Refraction Tomography and Resistivity Imaging to the Same Geologic Environment: A Case Study of Zaria Basement Complex in North Central Nigeria," *International Journal of Environmental, Ecological, Geological and Mining Engineering*, vol. 8, no. 10, pp. 624–627, 2014.

[31] M. Fkirin, A. Fkirin, S. Badawy, and M. F. El Deery, "Seismic Refraction Method to Study Subsoil Structure," *Journal of Geology & Geophysics*, vol. 5, no. 5, Jan. 2016, https://doi.org/10.4172/2381-8719.1000259.

[32] D. R. Hiltunen and B. J. Cramer, "Application of Seismic Refraction Tomography in Karst Terrane," *Journal of Geotechnical and Geoenvironmental Engineering*, vol. 134, no. 7, pp. 938–948, Jul. 2008, https://doi.org/10.1061/(ASCE)1090-0241(2008)134:7(938).

[33] G. Leucci, F. Greco, L. De Giorgi, and R. Mauceri, "Three-dimensional image of seismic refraction tomography and electrical resistivity tomography survey in the castle of Occhiolà (Sicily, Italy)," *Journal of Archaeological Science*, vol. 34, no. 2, pp. 233–242, Feb. 2007, https://doi.org/10.1016/j.jas.2006.04.010.

[34] S. T. G. Raghu Kanth and R. N. Iyengar, "Estimation of seismic spectral acceleration in Peninsular India," *Journal of Earth System Science*, vol. 116, no. 3, pp. 199–214, Jun. 2007, https://doi.org/10.1007/s12040-007-0020-8.

[35] M. L. Rucker, "Applying the seismic refraction technique to exploration for transportation facilities," *Geophysics*, pp. 1–18, Jan. 2000.